ELSEVIER

Available online at www.sciencedirect.com
ScienceDirect

Microporous and Mesoporous Materials xxx (2007) xxx–xxx

MICROPOROUS AND MESOPOROUS MATERIALS

www.elsevier.com/locate/micromeso

High temperature thermal expansion behavior of silicalite-1 molecular sieve: in situ HTXRD study

D.S. Bhange, Veda Ramaswamy *

Catalysis Division, National Chemical Laboratory, Pune 411008, India

Received 21 November 2006; received in revised form 5 February 2007; accepted 5 February 2007

Abstract

The measurement of the thermal expansion behavior of silica polymorph of zeolite MFI (Silicalite-1) was carried out in greater detail in the temperature range 373 K–673 K using high temperature X-ray diffraction (HTXRD) technique. The sample shows negative thermal expansion (NTE) in the temperature range studied, which is related to the transverse vibrations of the bridging oxygen atom between the two rigid polyhedrons. There is an anisotropy in the negative thermal expansion of this material that is contracting more along *a* axis than along the *b* and *c* axes. The bond angles and bond distances were determined from the Rietveld refinement data to look for any structural changes taking place as a function of temperature. The Si–O bond distances seem to play no role in the NTE, as there is no change in their distances as a function of temperature. It was observed that the Si–Si non-bonding distances for which the interatomic vectors are parallel to any of the crystallographic axes is responsible for the negative thermal expansion along the respective axes. The strong anisotropy in the expansion along *a* axis as compared to *b* and *c* directions is likely due to the stacking of the 2-dimensional layers in the *bc* direction. The observed decrease in Si–Si non-bonding distances with the constituent Si–O bond distances remaining constant, supports the correlation that the transverse vibrations of the bridging oxygen atoms in the structure are responsible for the NTE in this material.

© 2007 Elsevier Inc. All rights reserved.

Keywords: Silicalite-1; Rietveld refinement; HTXRD; Negative thermal expansion

1. Introduction

Research interest is increasing day by day in the materials exhibiting negative thermal expansion (NTE) i.e., materials which contract on heating. This phenomenon arises due to the secondary structural or dynamic mechanisms taking place during heating, that makes the normal thermal expansivity of chemical bonds ineffective. $BaTiO_3$ and $PbTiO_3$ like materials exhibit this phenomenon only when they are not in cubic phase and hence lead to anisotropy in thermal contraction [1]. The compounds like cordierite ($Mg_2Al_2Si_5O_{18}$) and NZP ($NaZr_2(PO_4)_3$) show very low negative thermal expansion [2]. This phenomenon is due to the rotation of the polyhedra, due to the thermal expansion of certain bonds in one or two dimensions. Another accepted mechanism for negative thermal expansion is the transverse thermal motion of two-coordinated cation/anion. Compounds having two-coordinated cations in their structure are very rare. Cu_2O is one of the examples of this type, which shows NTE below room temperature (RT) and positive thermal expansion above RT. The other oxidic materials, which show NTE, are microporous materials encompassing silicate zeolites and aluminophosphates. Zeolitic and $AlPO_4$ material show negative thermal expansion at high temperatures due to the transverse thermal motion of the two-coordinated oxygen atoms. In all these framework structures, dynamic rocking of essentially rigid polyhedra may be responsible for their thermal behavior. The transverse vibrations of these oxygen atoms can outweigh the expansion of the Si–O individual bonds and lead

* Corresponding author. Tel.: +91 20 2590 2012; fax: +91 20 2590 2633.
E-mail address: v.ramaswamy@ncl.res.in (V. Ramaswamy).

1387-1811/$ - see front matter © 2007 Elsevier Inc. All rights reserved.
doi:10.1016/j.micromeso.2007.02.013

to a decrease in the distances between the two Si atoms connected to the same oxygen atom. The powder diffraction studies on ($Sc_2(WO_4)_3$) [3] and a couple of zeolitic systems relates the contraction mechanism to the transverse vibrations of the two-coordinate bridging oxygens. The mechanism for the negative thermal expansion observed over large temperature region is yet unclear.

The reports including the studies of ITQ-1, ITQ-3, and SSZ-23 [4], ITQ-4 i.e., IFR [5,6], faujasite [7], MFI [8–10] and FER [11] showed that these materials exhibit strong negative thermal expansion on heating. Computational studies [12–14] have predicted the probable new materials that show contraction of the lattice on heating. Recently, we have reported that silicalite-1 and zirconium silicalite-1 molecular sieves having MFI type structure has shown large negative thermal expansion at high temperature ranges [9]. Strength of NTE of the material of MFI type is affected by isomorphous substitution of Si by heteroatom [15]. Hydrated and dehydrated HZSM-5 has different thermal behavior at high temperatures [16]. As MFI types of materials are having tunable catalytic properties for several commercial applications, we have selected this material for their negative thermal expansion studies.

In the present studies, we have studied the negative thermal expansion in silicalite-1 molecular sieve in the range 373–673 K. Full Rietveld analysis has been carried out to look in to the changes taking place in the bond distances and bond angles of the framework as a function of temperature, to explain the NTE behavior in this type of material.

2. Experimental

2.1. Sample preparation

Silicalite-1 (silica polymorph of ZSM-5 with MFI structure) used in the present work was prepared by the hydrothermal method (using sodium silicate as the silica source) published elsewhere [17]. The crystallization was carried out at 433 K for 48 h, under static conditions. After the crystallization, the solid product was filtered, washed with deionized water, dried at 383 K and calcined in air at 823 K for 16 h.

2.2. High temperature X-ray diffraction

High temperature X-ray diffraction (HTXRD) patterns in air were collected on the Philips X'Pert Pro 3040/60 diffractometer equipped with Anton Parr HTK 1600 attachment. A small amount of silicon (NIST, $a = 5.4311$ Å) as an internal standard was added to the sample. The sample thickness was ~0.5 mm which was mounted on a platinum strip (cavity), which serves as the sample stage as well as the heating element. A Pt/Rh-13% thermocouple spot-welded to the bottom of the stage was used for measuring the temperature. α-Al_2O_3 standard (NIST, Gaithersberg, USA) was used for the calibration of the high temperature stage. The HTXRD patterns for silicalite-1 sample in the temperature range 373–673 K were collected in the 2θ region 10–60° in the continuous mode with a step size of 0.0167 and a time 20 s/step using Ni filtered Cu Kα radiation ($\lambda = 1.5406$ Å) and X'celerator as detector. Diffraction patterns were collected at every 50 K interval. A heating rate of 10 K min^{-1} and a soak time of 10 min were applied. Bragg–Brentano geometry was employed. The optics used in the incident beam (primary) were 0.04 radian soller slit, 1/2° divergence slit and 10 mm mask, and 0.02 radian soller slit in the secondary beam path.

2.3. Rietveld analysis

Collected HTXRD patterns were refined using the Rietveld method [18]. The unit cell parameters at each temperature were refined with the Rietveld method using the GSAS [19] package and the EXPGUI graphical interface [20], which allows proper treatment of the instrumental aberration parameters, such as the goniometer shift and the sample displacement parameters. The goniometer zero correction was applied with respect to Si as standard, and the sample displacement as a function of temperature was determined manually from the Si reflection (1 1 1) at different temperatures. The starting atomic coordinates for the MFI in the orthorhombic phase (space group Pnma (62)) were taken from Ref. [21]. It was decided to exclude the reflections from Pt and Si rather than model them as additional phases in the diffraction patterns. The pseudo-Voigt peak profile function, with up to 17 refinable parameters, was chosen and the peaks were truncated at 0.01% of the peak maxima. Background intensity was modeled by a Chebyshev type I polynomial function with 16 background parameters. An overall scale factor, the cell parameters, and the sample displacement parameter were simultaneously refined. Because of the complexity of the structure, soft restraints were applied to Si–O bond distances (1.59 ± 0.05 Å) with a suitable weighting factor, which was gradually reduced as the refinement proceeded. Framework atoms of the same element type were constrained to have the same isotropic thermal displacement parameters. While the thermal expansion coefficient along the three crystallographic directions a, b and c were calculated for all the scans using the formulae $\alpha_a = \Delta a/(T - RT)a_{RT}$, $\alpha_b = \Delta b/(T - RT)b_{RT}$ and $\alpha_c = \Delta c/(T - RT)c_{RT}$, respectively, the lattice or volume thermal expansion coefficient was calculated using the formula $\alpha_V = \Delta V/(T - RT)V_{RT}$ where T and RT are the typical temperature of the scan and room temperature, respectively; Δa, Δb, Δc and ΔV are the differences in the values of the respective unit cell parameters of the scans at T and RT.

3. Result and discussions

Temperature resolved PXRD patterns collected over the temperature range 373–673 K in 50 K intervals are shown in Fig. 1. From Fig. 1, it is clear that silicalite-1 material under examination shows orthorhombic phase in the tem-

Please cite this article in press as: D.S. Bhange, V. Ramaswamy, Micropor. Mesopor. Mater. (2007), doi:10.1016/j.micromeso.2007.02.013

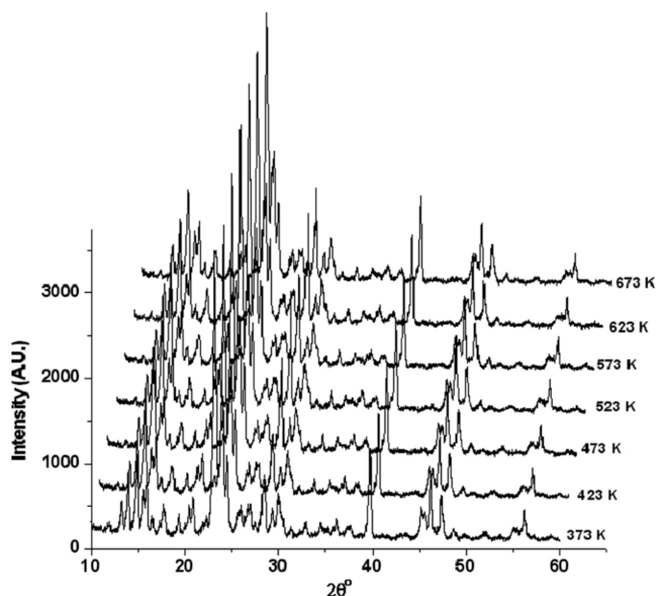

Fig. 1. Multiple plot of powder XRD patterns of silicalite-1 as a function of temperature scanned in air from 373 to 673 K at 50 K intervals.

perature range studied corroborating with the literature data. The data quality of the scan is comparatively good due to the X'celerator detector, which uses the RTMS (real time multiple strip) technology enhancing both the resolution and intensity of the reflections. We do not observe any phase transition in the temperature range 373–673 K.

Information regarding unit cell parameters as a function of temperature is extracted from Rietveld refinement technique. Quality of the Rietveld refinement is monitored through *Rp*-values from the fit. The agreement between the experimental and the simulated diffraction patterns is shown in Fig. 2. All the details of the Rietveld refinement at 373 K are listed in Table 1. *Rwp* values for all the fits were below 10.0%. Unit cell parameters obtained from Rietveld refinement technique have been plotted as a function of temperature, which is shown in Fig. 3. These values

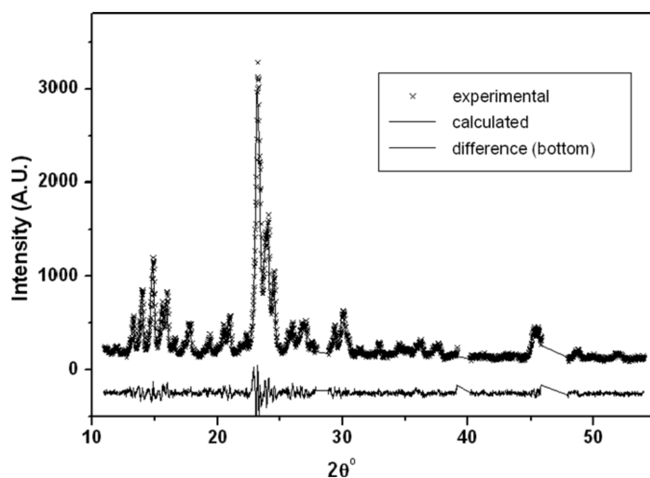

Fig. 2. Rietveld refinement of the powder XRD pattern collected at 673 K, showing the experimental, calculated and difference plots.

Table 1
Crystallographic data and experimental conditions for the Rietveld refinement of silicalite-1 (scan at 373 K scan)

Sample	Silicalite-1
Formula	$Si_{96}O_{192}$
Crystal system	Orthorhombic
Space group	Pnma
a (Å)	20.087(2)
b (Å)	19.875(2)
c (Å)	13.383(2)
V (Å^3)	5342.82(9)
λ (Å)	1.5406
2θ Range (°)	10–60
Step size (° 2θ)	0.0167
No. of data points	2342
R_p (%)	7.52
R_{wp} (%)	9.52
Red. χ^2	2.72
Background function	Shifted Chebyshev 16-coefficients
Profile function	Pseudo-Voigt

at different temperatures were used in the further calculations of thermal expansion coefficients. Although there is no appreciable change in the unit cell volume in the temperature range 373–423 K, yet there is contraction along *a* axis, expansion along *b* axis and no change in the *c* direction. In the temperature range 473–673 K, the thermal contraction is anisotropic along the three crystallographic axes. The extent of thermal contraction along *a* (0.026 Å) axis is comparatively more than along *b* (0.005 Å) and *c* (0.010 Å) axes. Unit cell volume in the overall temperature range 373–673 K decreased from 5342.80 to 5330.64 Å^3. The thermal expansion coefficient calculated according to the formula used in literature [9] along *a* axis (α_a) is $-4.314 \times 10^{-6}\ K^{-1}$. The thermal expansion along *b* axis is marginal as compared to *a* axis. The thermal expansion coefficients along *b* axis and along *c* axis (α_b) are $-0.838 \times 10^{-6}\ K^{-1}$ and $(\alpha_c) = -2.490 \times 10^{-6}\ K^{-1}$, respectively. Lattice thermal expansion coefficient (α_v) in the overall temperature range 373–673 K is $-7.586 \times 10^{-6}\ K^{-1}$. Fig. 4 shows the plot of 2θ shift due to sample displacement with respect to temperature, which shows a systematic increase in sample displacement as the temperature increases.

Refinement of the fractional coordinates of the constituent atoms has been carried out to observe the changes in the structure as a function of temperature. The results from the Rietveld refinement of the XRD patterns at seven temperatures between 373 and 673 K in steps of 50 K enabled us to gain more insight into the structural changes responsible for the negative thermal expansion in silicalite-1. MFI framework in the *Pnma* space group has twenty-six Si–O–Si bonds present in the unit cell. The bond angles and bond distances were calculated from the final refinement data to look for any change with respect to increase in temperature. Fig. 5 shows changes in Si_1–O distances as a function of temperature. There is no appreciable change in the Si_1–O bond distances as a function of temperature. These changes in Si–O distances are nearly equal to the estimated

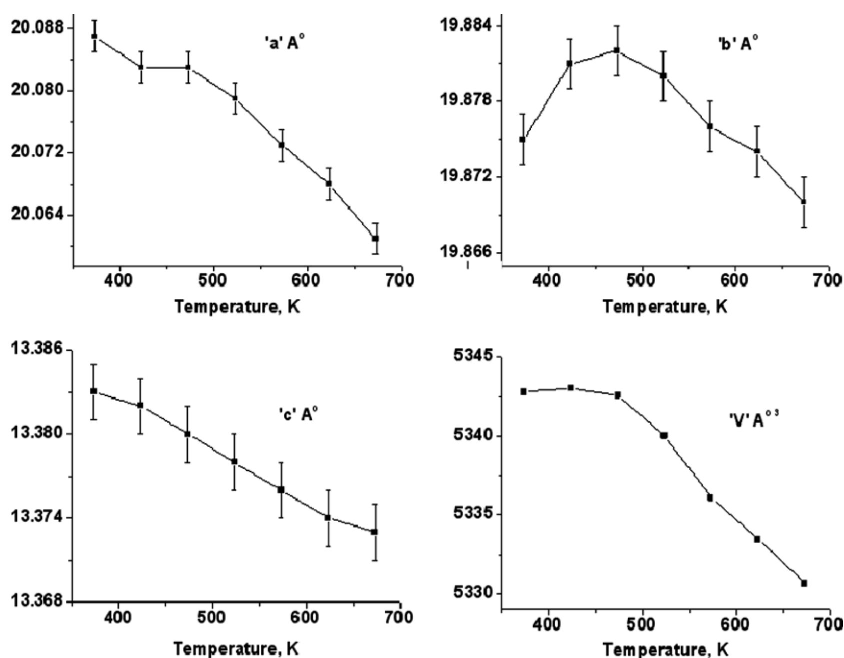

Fig. 3. Variation of unit cell parameters *a* (Å), *b* (Å), *c* (Å) and '*V*' (Å^3) with temperature for silicalite-1.

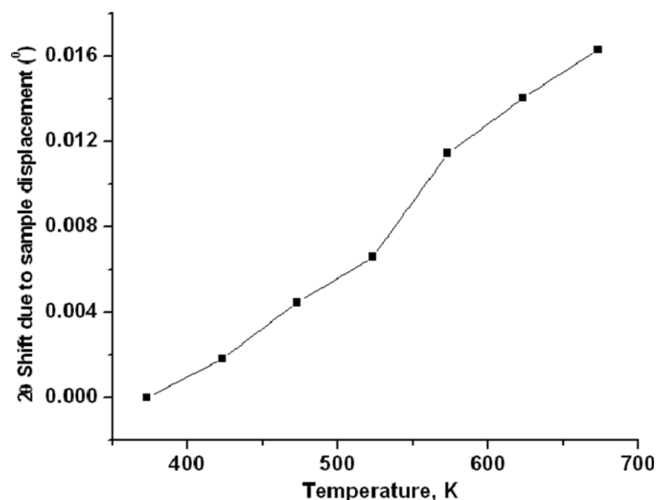

Fig. 4. 2θ° Shift due to sample displacement as a function of temperature.

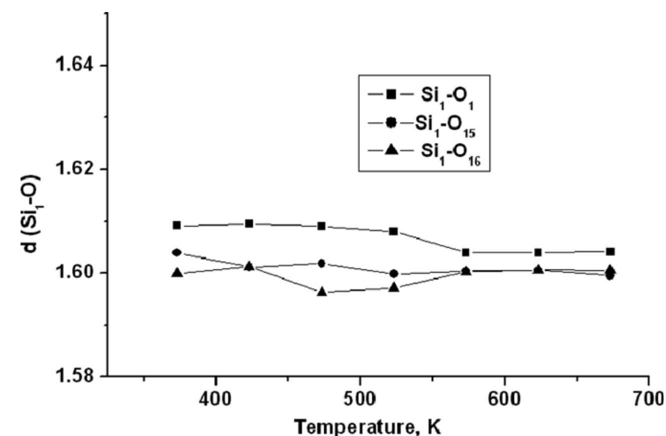

Fig. 5. Variation of different Si_1–O bond distances as a function of temperature.

standard deviation (0.002Å) of the Rietveld refinement. The changes in the average Si_1–O bond distances and averaged Si–O–Si bond angle as a function temperature are plotted in Fig. 6. There is no regular trend in the change in Si–O–Si bond angles hence we have averaged them, which decreases from 153° to 149°. The average Si_1–O distance remains approximately constant as a function of temperature. All other Si_n–O (where $n = 1$ to 12) bonds show fairly same trend in their behavior. Hence, changes in Si–O bond distances do not seem to be responsible for the contraction of the framework.

Changes in Si–Si non-bonding distances as a function of temperature may affect the three crystallographic axes and the change is more predominant when its inter atomic vector has its major component parallel. Orientation of the Si–Si vectors with the crystallographic axis is calculated from taking the cosine function of the angle made by Si–O–Si bond with that axis. A change in the particular Si–O–Si bond angle can be said to strongly contribute to a change in that axis if $\cos\theta$ is greater than $\sim$0.7(i.e., $\theta < \sim 45°$) as suggested by Bull et.al. [10]. Angle made between each of Si–O–Si vectors and three crystallographic axes in silicalite-1 in P*nma* space group are listed in Table 2 along with the calculated $\cos\theta$ values. Along the crystallographic axis *a*, there are eight Si–Si distances ($\cos\theta > 0.7$), for which the inter atomic vectors are having their major components parallel to *a* axis. The bond distances Si_3–Si_{12}, Si_4–Si_5, Si_4–Si_7, Si_7–Si_7, Si_9–Si_9, Si_{10}–Si_{10}, Si_{10}–Si_{11} and Si_{12}–Si_{12} are the distances for which major components of the Si(O)Si interatomic vectors are parallel to *a* axis.

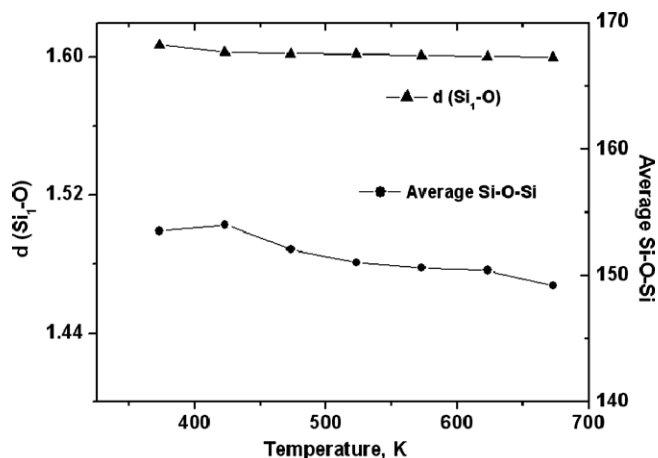

Fig. 6. Average changes in d (Si_1–O) and Si–O–Si bond angles with temperature.

There is decrease in d (Si–Si) for the Si_3–Si_{12}, Si_4–Si_7, Si_7–Si_7, Si_{10}–Si_{11} and Si_{12}–Si_{12} and the major decrease in d (Si–Si) is for Si_7–Si_7 (0.14 Å) and Si_{12}–Si_{12} (0.086Å). The changes in some of these Si–Si non-bonding distances are given in Fig. 7a, which show a major change in d (Si–Si) as a function of temperature. Along b axis there are also eight Si–Si non-bonding distances, for which the inter atomic vectors have their major components parallel to b axis and these distances are Si_1–Si_2, Si_1–Si_5, Si_2–Si_3, Si_5–Si_6, Si_7–Si_8, Si_7–Si_{11}, Si_8–Si_9 and Si_{11}–Si_{12}. There is an expansion in the lattice along b axis as a function of temperature from 373 to 423 K. The non-bonding distances of Si_1–Si_5, Si_2–Si_3 and Si_{11}–Si_{12} whose vector components are parallel to b axis increase as a function of temperature. The major changes are seen only in the distances of the Si_7–Si_8 (0.039 Å) and Si_{11}–Si_{12} (0.116 Å), which are increasing, and Si_5–Si_6 (0.078 Å) and Si_8–Si_9 (0.095 Å), which are decreasing, as a function of temperature in the range 373–673 K (Fig. 7b). Along the c axis there are only four Si–Si distances, for which the inter atomic vectors have their major components oriented parallel to the c axis. The non-bonding distance of the Si_3–Si_4 and Si_9–Si_{10} increases as a function of temperature, while there is a decrease in the non-bonding distances of the Si_2–Si_8 and Si_5–Si_{11} (Fig. 7c), which may cause the contraction along the c axis.

One of the reasons for the anisotropy in the negative thermal expansion behavior in silicalite-1 along three crystallographic axes is likely due to the layered structure of the MFI material. In MFI type of material there is stacking of the two dimensional layer along a axis (Fig. 8a). This two dimensional layer is in bc plane (Fig. 8b and c). This stacking makes silicon atoms to be more denser along b and c directions as compared to a direction. This dense Si portions may be acting as condensed matter and resisting to contract, while there is greater porous portion along a axis than dense portion and hence Si framework may be getting easily contracted. Hence, there may be more reduction along the axis in which there is stacking of these layers in the bc plane. The thermal behavior of the ferrierite material studied so far in the literature [11] can also be explained in the same way. Ferrierite material has a layered structure. These layers are in the ab direction and are stacked along c axis and a large contraction in the c axis in that material as compared to a and b axes is reported. Sleight [22] also describes anisotropic thermal expansion in corderite and β-eucryptite in the same way. In both corderite and β-eucryptite, there are layers of polyhedra, which expands horizontally (ab direction) and as the layers undergo thermal expansion, they are pulled together in the other directions; as a result there is contraction along c direction.

The bond angles and bond distances in SiO_4 remain unchanged in the temperature range studied indicating the rigid tetrahedral nature of SiO_4 units. From these results, one can conclude that the negative thermal expansion of silicalite-1 is related to the transverse vibrations of the two-coordinate bridging oxygen atoms, a mode of lattice vibration, which can easily get excited with low energy input. This can induce a coupled rotation of the essentially rigid SiO_4 tetrahedra. There are no systematic changes in refined atomic coordinates and bond angles calculated in the present study. The Si–Si distances decrease due to the transverse vibration of two corner sharing oxygen atoms, and the constituent Si–O bond distance remain approximately constant. These vibrations can take place in a correlated fashion as phonon modes that do not change Si–O bond length but do excite transverse Si–O–Si vibrations, which are called rigid unit modes (RUM) [23]. This confirms that presence

Table 2
Angles θ and $\cos\theta$ made between each of the Si(O)Si vectors and the three crystallographic axes

Bonds	θ_a	θ_b	θ_c	$\cos\theta_a$	$\cos\theta_b$	$\cos\theta_c$
Si_1–O_1–Si_2	59.18	39.50	67.85	0.512	*0.772*	0.377
Si_2–O_2–Si_3	49.45	45.17	73.55	0.650	*0.705*	0.283
Si_3–O_3–Si_4	88.89	89.31	1.30	0.019	0.012	*0.999*
Si_4–O_4–Si_5	19.20	84.66	71.62	*0.944*	0.093	0.315
Si_5–O_5–Si_6	79.13	32.68	59.60	0.188	*0.842*	0.506
Si_2–O_6–Si_6	54.04	55.09	55.08	0.587	0.572	0.572
Si_7–O_7–Si_8	67.00	23.34	86.22	0.391	*0.918*	0.066
Si_8–O_8–Si_9	81.23	20.14	72.02	0.152	*0.939*	0.309
Si_9–O_9–Si_{10}	89.67	86.40	3.61	0.006	0.063	*0.998*
Si_{10}–O_{10}–Si_{11}	32.40	69.42	66.14	*0.844*	0.352	0.404
Si_{11}–O_{11}–Si_{12}	89.76	25.19	64.81	0.004	*0.905*	0.426
Si_8–O_{12}–Si_{12}	53.78	50.16	60.63	0.591	0.641	0.490
Si_2–O_{13}–Si_8	79.13	89.04	10.91	0.189	0.017	*0.982*
Si_5–O_{14}–Si_{11}	52.40	89.13	37.62	0.610	0.015	*0.792*
Si_1–O_{15}–Si_{10}	48.89	72.93	46.06	0.657	0.293	0.694
Si_1–O_{16}–Si_4	58.79	50.49	55.14	0.518	0.636	0.572
Si_4–O_{17}–Si_7	17.72	74.04	82.50	*0.952*	0.275	0.130
Si_6–O_{18}–Si_9	48.12	70.71	48.14	0.666	0.330	0.667
Si_3–O_{19}–Si_6	58.86	51.95	53.57	0.517	0.616	0.594
Si_3–O_{20}–Si_{12}	27.33	64.83	80.04	*0.888*	0.425	0.173
Si_1–O_{21}–Si_5	77.77	23.47	70.29	0.212	*0.917*	0.337
Si_7–O_{22}–Si_{11}	74.08	16.27	86.75	0.274	*0.960*	0.057
Si_7–O_{23}–Si_7	10.89	90.00	79.11	*0.982*	0	0.188
Si_{12}–O_{24}–Si_{12}	3.33	90.00	86.67	*0.998*	0	0.058
Si_9–O_{25}–Si_9	35.45	90.00	54.55	*0.815*	0	0.580
Si_{10}–O_{26}–Si_{10}	29.99	90.00	60.01	*0.866*	0	0.499

Please cite this article in press as: D.S. Bhange, V. Ramaswamy, Micropor. Mesopor. Mater. (2007), doi:10.1016/j.micromeso.2007.02.013

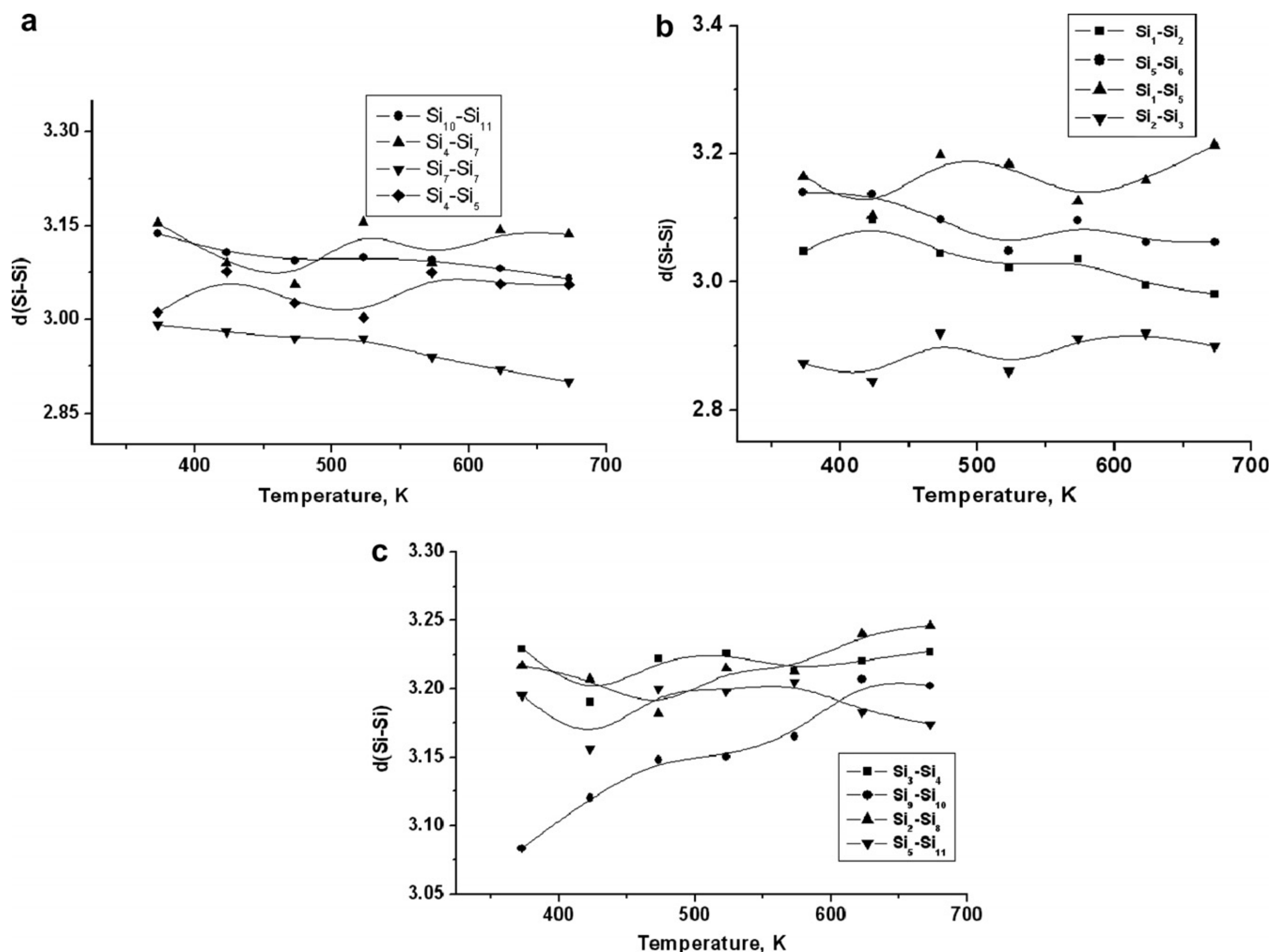

Fig. 7. Variation in the Si–Si non-bonding distances as a function of temperature. The three graphs (a)–(c) show those vectors, which are having their largest components parallel to the three crystallographic axes *a*, *b* and *c*, respectively.

of rigid unit modes are responsible for the NTE observed in silicalite-1. To correlate the changes in individual Si–O–Si angles with the associated Si–O bond lengths as a function of temperature, a typical plot is shown in Fig. 9 for a set of two bond lengths Si_1–O_1 and Si_2–O_1 along with the Si_1–O_1–Si_2 bond angle. It shows that the bond length is approximately constant while the bond angles decreases, supporting the presence of rigid unit modes. The variation in the trend seen in the temperature range 473–573 K could be probably due to the displacive phase transformation within the same space group or any other mechanism. From the Fig. 7a–c, one can conclude that the Si–Si non-bonding distances decreases as a function of temperature. This decrease in the Si–Si non-bonding distances is a result of the transverse vibrations of bridging oxygen atoms (two fold coordination) between two rigid polyhedrons, which is responsible for the NTE observed. This is also discussed as intrinsic mechanism of negative thermal expansion in the literature [16]. The high temperature thermal behavior of the material of this type is also explained by molecular dynamic simulation studies, which also infers that the bending of Si–O–Si linkages and rotation of SiO_4 tetrahedra play an important role in NTE [24]. After refinement of powder patterns collected at 373 and 673 K, we have measured the distance between O_5–O_{11} and O_{21}–O_{22} atoms in the rings using Diamond 2.1c software. The dimensions of the straight channel showed a decrease with increase in temperature, which is pictorially illustrated in Fig. 10. The distance between the O_5–O_{11} and O_{21}–O_{22} decreases as a function of temperature from 8.339 Å and 8.286 Å to 7.999 Å and 8.245 Å, respectively.

4. Conclusions

In situ HTXRD studies on silicalite-1 with MFI structure were carried out over the temperature range 373–673 K at 50 K intervals. Rietveld refinements of the HTXRD patterns collected were done to see any structural changes as a function of temperature. Lattice thermal expansion coefficient in the temperature range studied is $-7.586 \times 10^{-6}\,K^{-1}$ and thermal behavior of the material is anisotropic in the temperature range studied. There was more contraction along *a* axis as compared to *b* and *c* axes. The stacking of 2-dimensional layers along the crystallographic

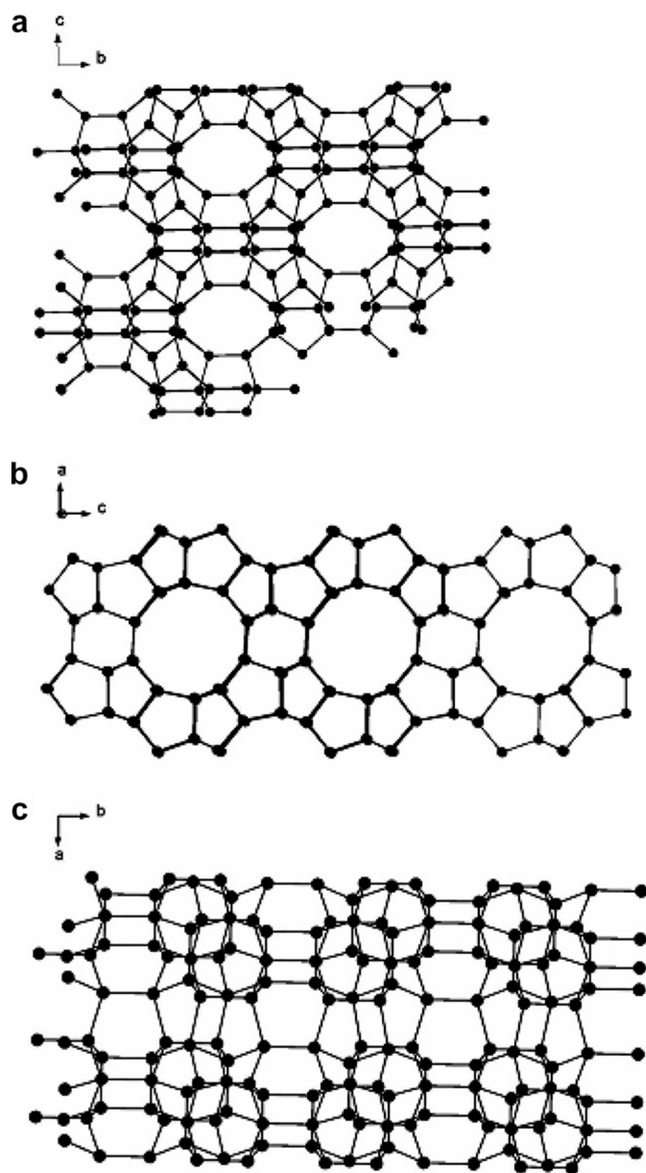

Fig. 8. Framework topology of silicalite-1 having MFI structure. The silicon atoms are shown in black and oxygen atoms are not shown for sake of clarity: (a) shows the view along 1 0 0 axis, (b) shows the view along 0 1 0 axis and (c) shows the view along 0 0 1 axis.

direction *a* explains the strong anisotropy in the expansion along that direction. No change in the Si–O bond distances indicates that they are not playing any role in the contraction mechanism leading to negative thermal expansion of this material. The transverse vibrations of the Si–O–Si bridging oxygen atoms decreases the Si–Si non-bonding distances which causes the contraction in the material as a function of temperature. These vibrations seem to take place in a correlated fashion as phonon modes, which excite transverse Si–O–Si vibrations but do not change Si–O bond distances. The individual Si–Si non-bonding distances which vary as a function of temperature and whose interatomic vectors are parallel to any one of the crystallographic axes are likely to be responsible for the thermal behavior of the sample along the respective axes.

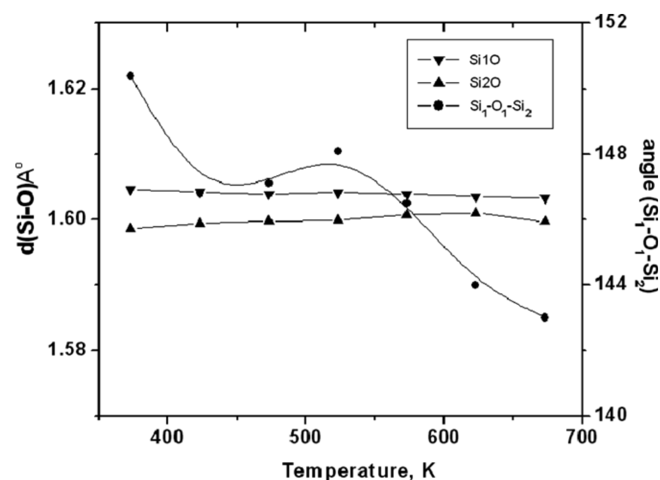

Fig. 9. The changes in individual Si_1–O_1–Si_2 angles with the associated Si–O_1 bond lengths as a function of temperature.

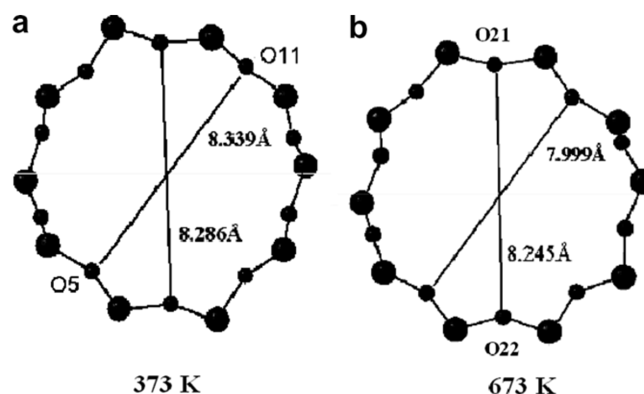

Fig. 10. Pictorial representation of how the rings and cavities change dimension with temperature (straight channel) are shown for the sample scanned at (a) 373 K and (b) 673 K.

Acknowledgements

One of the authors (D.S.B.) thanks UGC, New Delhi, India for research fellowship.

References

[1] G. Shirane, S. Hoshina, J. Phys. Soc. Jpn. 6 (1951) 265.
[2] D.A. Woodcock, P. Lightfoot, C. Ritter, Chem. Commun. 1 (1998) 107.
[3] J.S.O. Evans, T.A. Mary, A.W. Sleight, J. Solid State Chem. 137 (1998) 148.
[4] D.A. Woodcock, P. Lightfoot, P.A. Wright, L.A. Villaescusa, M.J. Díaz-Cabañas, M.A. Camblor, J. Mater. Chem. 9 (1999) 349.
[5] D. A Woodcock, P. Lightfoot, L.A. Villaescusa, M.J. Díaz-Cabañas, M.A. Camblor, D. Engberg, Chem. Mater. 11 (1999) 2508.
[6] L.A. Villaescusa, P. Lightfoot, S.J. Teat, R.E. Morris, J. Am. Chem. Soc. 123 (2001) 5453.
[7] M.P. Attfield, A.W. Sleight, J.C.S. Chem. Commun. 5 (1998) 601.
[8] S.H. Park, R.W. Grosse Kunstleve, H. Graetsch, H. Gies, Stud. Surf. Sci. Catal. 105 (1997) 1989 [Progress in Zeolites and Microporous materials Ed. by H.Chon, S.-K. Ihm and Y.S. Uh].
[9] D.S. Bhange, V. Ramaswamy, Mater. Res. Bull. 41 (2006) 1392.

[10] I. Bull, P. Lightfoot, L.A. Villaescusa, L.M. Bull, R.K.B. Gover, J.S.O. Evans, R.E. Morris, J. Am. Chem. Soc. 125 (2003) 4342.
[11] B.A. Marinkovic, P.M. Jardim, A. Saavedra, L.Y. Lau, C. Baehtz, R.R. de Avillez, F. Rizzo, Micropor. Mesopor. Mater. 71 (2004) 117.
[12] P. Tschaufeser, S.C. Parker, J. Phys. Chem. 99 (1995) 10609.
[13] J.W. Couvest, R.H. Jones, S.C. Parker, P. Tschaufeser, C.R.A. Catlow, J. Phys. Condens. Matter. 5 (1993) L329.
[14] J.D. Gale, J. Phys. Chem. B 102 (1998) 5423.
[15] D.S. Bhange,V. Ramaswamy, Mater. Res. Bull. (2006), doi:10.1016/j.materresbull.2006.08.024.
[16] P.M. Jardim, B.A. Marinkovic, A. Saavedra, L.Y. Lau, C. Baehtz, F. Rizzo, Micropor. Mesopor. Mater. 76 (2004) 23.
[17] R. Szoztak, T.L. Thomas, J. Catal. 100 (1986) 555.
[18] H.M. Rietveld, Acta. Crystallogr. 22 (1967) 151;
J. Appl. Crystallogr. 2 (1969) 65.
[19] A.C. Larson, R.B. von Dreele, GSAS Generalized strucure analysis system, Laur 86-748, Los Alamos National Laboratory, Los Alamos, New Mexico, 1994.
[20] B. Toby, J. Appl. Cryst. 34 (2001) 210.
[21] H. van Koningsveld, H. van Bekkum, J.C. Jansen, Acta Cryst. B 43 (1987) 127;
G. Artioli, C. Lamberti, G.L. Marra, Acta Cryst. B56 (2000) 2.
[22] A.W. Sleight, Inorg. Chem. 37 (1998) 2854.
[23] A. Bieniok, K.D. Hammonds, Micropor. Mesopor. Mater. 25 (1998) 193.
[24] S. Sen, R.R. Wusirika, R.E. Youngman, Micropor. Mesopor. Mater. 87 (2006) 217.

Please cite this article in press as: D.S. Bhange, V. Ramaswamy, Micropor. Mesopor. Mater. (2007), doi:10.1016/j.micromeso.2007.02.013